

Microwave-assisted synthesis and photodynamic activity of tris-heteroleptic Ru(II) complexes with asymmetric polypyridyl ligands

Ilona Gurgul^a, Olga Mazuryk^{a,*}, Dorota Rutkowska-Zbik^b, Michał Łomzik^c, Aneta Krasowska^a, Piotr Pietrzyk^a, Grażyna Stochel^a, Małgorzata Brindell^a

^a Department of Inorganic Chemistry, Faculty of Chemistry, Jagiellonian University in Kraków, Gronostajowa 2, 30-387 Krakow, Poland

^b Jerzy Haber Institute of Catalysis and Surface Chemistry, Polish Academy of Sciences, Niezapominajek 8, 30-239 Krakow, Poland

^c Department of Organic Chemistry, Faculty of Chemistry, University of Łódź, ul. Tamka 12, 91-403 Łódź, Poland

ARTICLE INFO

Keywords:

Heteroleptic ruthenium(II) complexes
Tris-bidentate complexes
Microwave-assisted synthesis
Cytotoxicity
Photocytotoxicity
ROS

ABSTRACT

Ru(II) polypyridyl complexes are attracting particular attention as possible photodynamic therapy (PDT) agents due to their interesting photophysical properties, which can be easily tunable through the appropriate selection of attached ligands. However, blue-wavelength absorption of the complexes limited their potential application. In this study, three tris-heteroleptic Ru(II) polypyridyl complexes were synthesized to shift the absorption of the compounds toward longer wavelengths. Their photophysical, biological, and photodynamic properties were evaluated. The mechanism of the photoinduced toxicity was investigated by fluorescence and electron paramagnetic resonance (EPR) techniques *in vitro* and in aqueous solutions. The results revealed the photodynamic activity of the studied compounds is based mainly on the photogeneration of ¹O₂ and H₂O₂. Additionally, the synthesized Ru complexes demonstrated high activity in inhibiting the detachment of cancer cells. This effect was additionally enhanced by light activation of Ru compounds. The presented findings demonstrate a rational strategy for the efficient synthesis of tris-heteroleptic Ru(II) polypyridyl complexes to be used as promising photodynamic agents for cancer and antimetastatic treatments.

1. Introduction

Photodynamic therapy (PDT) has emerged as a promising alternative cancer treatment or complement to chemotherapy, radiotherapy, or surgery. The success of PDT is attributed to its excellent spatial and temporal selectivity, negligible side effects, and non-invasiveness [1]. PDT is based on the excitation of generally nontoxic photosensitizers (PS) in the dark with visible or near-infrared light to alter the viability of cancer cells by, among others, generating high levels of reactive oxygen species (ROS) [2]. The production of ROS occurs because of energy or electron or hydrogen atom transfer from the triplet excited state of the

PSs to dioxygen molecule. Therefore, compounds with long-lived triplet excited states are desirable for PDT.

Ruthenium(II) polypyridyl complexes are drawing particular attention because of their rich photophysical and outstanding biological properties. In addition to PDT, Ru complexes are used in photochemotherapy [3–7], imaging [8–11], or solar energy conversion [12,13], among others. The most successful Ru(II) compound TLD-1433 has recently entered phase II clinical trials as a photosensitizer for PDT against bladder cancer [14,15]. Ruthenium(II) polypyridyl complexes possess a long list of advantages, which makes them a promising alternative for currently used therapeutics. Researchers often mention

Abbreviations: CAN, acetonitrile; APF, aminophenyl fluorescein; Bpy, 2,2'-bipyridine; DCF, 2',7'-dichlorofluorescein; DFT, density functional theory; dip, 4,7-diphenyl-1,10-phenanthroline; DMF, dimethylformamide; DMPO, 5-dimethyl-1-pyrroline N-oxide; DMSO, dimethyl sulfoxide; dpb, 2,3-bis(2-pyridyl)benzo[g]quinoxaline; DPBS, Dulbecco's phosphate-buffered saline; dpq, 2,3-bis(2-pyridyl)quinoxaline; EPR, electron paramagnetic resonance; FBS, fetal bovine serum; HE, hydroethidine; HPLC, high-pressure liquid chromatography; HRMS, high-resolution mass spectrometry; IC₅₀, inhibitory concentration; ICP-MS, inductively coupled plasma mass spectrometry; IEFPCM, integral equation formalism variant; IL, intra-ligand; ILCT, intra-ligand charge transfer; MLCT, metal-ligand charge transfer; PBS, phosphate-buffered saline; PCM, polarizable continuum model; PDT, photodynamic therapy; PI, photodynamic index; PS, Photosensitizer; PTLC, preparative thin-layer chromatography; ROS, reactive oxygen species; SOSG, singlet oxygen sensor green; TD-DFT, time-dependent – density functional theory; TLC, thin layer chromatography; TEMP, 2,2',6,6'-tetramethylpiperidine; TEMPO, 2,2',6,6'-tetramethylpiperidine-1-oxyl.

* Corresponding author.

E-mail address: mazuryk@chemia.uj.edu.pl (O. Mazuryk).

<https://doi.org/10.1016/j.poly.2022.116049>

Received 1 April 2022; Accepted 15 July 2022

Available online 20 July 2022

0277-5387/© 2022 The Author(s). Published by Elsevier Ltd. This is an open access article under the CC BY-NC-ND license (<http://creativecommons.org/licenses/by-nc-nd/4.0/>).

intense luminescence, large Stokes shift, high water solubility, and good photostability of Ru(II) polypyridyl complexes [16]. However, the longest-wavelength absorption band (usually a metal-to-ligand-charge-transfer MLCT transition) of most Ru(II) complexes is located in the blue region of the visible spectrum (<500 nm), which limits their phototherapeutic applications [17,18]. Therefore, exploring new Ru(II) compounds with absorption spectra closer to the 'therapeutic window' of 600–850 nm is highly desirable for PDT. To take advantage of the structure of Ru compounds and explore each ligand in their structure, tris-heteroleptic Ru(II) compounds need to be synthesized. The selection of the solvent to introduce the first ligand into this heteroleptic structure is crucial in synthesis [19]. Carrying out the reaction in protic solvents or solvents with high boiling points results in obtaining a mixture of homoleptic compounds [19]. The introduction of the second ligand is also demanding; classical synthesis often leads to low yields and very long reactions; therefore, studies on tris-heteroleptic Ru(II) complexes are relatively rare. To improve this process, we propose the use of microwave synthesis at this stage. The appropriate choice of the ligands determines not only the photophysical and physicochemical properties of the Ru(II) complexes (lipophilicity, stability, reactivity of the excited states) but also completely controls the biological properties of the compounds, such as cellular uptake and localization, accumulation route or cytotoxicity [20].

Currently, one of the main drawbacks of PDT is the dependence of its efficiency on the oxygen level in the treated tissues [21]. Since most of the explored PDT systems operate through the energy transfer process (type II sensitization mechanism) and rely on singlet oxygen generation, the use of such systems in hypoxic tumors is inherently limited. Therefore, the focus of newly developed compounds is shifting towards the development of photosensitizers, the photosensitization activity of which will be based on both energy and electron/hydrogen atom transfer processes [22,23].

This work focuses on the synthesis of three new tris-heteroleptic Ru(II) polypyridyl complexes. The 4,7-diphenyl-1,10-phenanthroline (dip) and 2,2'-bipyridine (bpy) ligands are chosen to ensure the appropriate biological properties of the complexes, while 2,3-bis(2-pyridyl)quinoxaline (dpq) and its derivatives were applied to shift the MLCT transition of the compounds towards longer wavelengths. The modification of the synthetic protocol with the use of microwave irradiation allowed us to reduce the reaction times and achieve high yields of the desired complexes. The complexes were synthesized as a mixture of isomers and separated with the use of preparative chromatography. The Ru(II) complexes were characterized with the use of DFT calculations. Biological evaluation was performed only for the prevalent isomer of each synthesized Ru complex. Stereoisomers of Ru(II) polypyridyl complexes may interact differently with chiral biomacromolecules such as DNA or proteins. However, several studies have shown that most often only modest differences (if any) in biological activities between stereoisomers can be observed [20]. The potential of the compounds as cyto- and photocytotoxic agents was evaluated against the highly aggressive breast cancer cell line MDA-MB-231. Based on our previous work [24], we speculate that even a subtle modification of the structure in one of the ligands may lead to a different excited state behavior and photobiological activity of a compound. Our goal was to determine the most photoreactive complex *in vitro* and investigate the basis of its photodynamic activity. Furthermore, the influence of irradiation on the antimetastatic activity of Ru(II) polypyridyl complexes was explored.

The presented studies showed that while the synthesized Ru(II) complexes differed in cytotoxic activity, irradiation with visible light greatly enhanced their antiproliferative properties. The phototoxicity of the compounds was caused by the generation of $^1\text{O}_2$ and H_2O_2 , which proved that the complexes can generate ROS via type I and II sensitization mechanisms. An additional benefit came from the enhanced antimetastatic activity of the Ru complexes upon visible light irradiation. This could provide the basis for exploring a potential combination of PDT and antimetastatic therapy using Ru(II) polypyridyl complexes.

2. Material and methods

2.1. Synthesis of complexes

2.1.1. Chemicals and instrumentation

All solvents were analytical grade and were used without further purification. The reagents were purchased from Sigma-Aldrich. 2,2'-bipyridine (bpy), 4,7-diphenyl-1,10-phenanthroline (dip) and 6,7-dimethyl-2,3-bis(2-pyridyl)quinoxaline (Me_2dpq) were purchased from Sigma-Aldrich, while two other ligands 2,3-bis(2-pyridyl)quinoxaline (dpq) and 2,3-bis(2-pyridyl)benzo[g]quinoxaline (dipb) were synthesized according to published procedures [25,26]. Chemical syntheses were performed using a professional microwave reactor (Anton Paar).

The purity was confirmed by a high-pressure liquid chromatography (HPLC) system (HPLC-DAD Shimadzu LC-2030C). Gradient elution was performed on a column C8-RP (Waters; Symmetry C8 5 μm) at 25 °C, using a mixture of ammonium acetate (0.1 M) and acetonitrile (50–95 %, 20 min) as a mobile phase at a flow rate of 1 ml/min.

HRMS spectra were recorded on a microTOF-Q II mass spectrometer (Bruker, Germany).

^1H NMR spectra were recorded at 294 K on a Bruker Avance III 600 MHz spectrometer at 600.3 MHz. The ^1H chemical shifts were calibrated based on the residual ^1H solvent peaks, i.e., $\delta = 3.31$ ppm for CD_3OD .

2.1.2. Synthesis of *cis*-[RuCl₂(DMSO)₄]

Synthesis was performed according to a procedure in the literature [27]. Ruthenium(III) chloride hydrate (1 g) was mixed with DMSO (6 ml) and heated to reflux (180 °C) for about one minute. After that, the volume of the solution was reduced to approximately half of the original. To the resulting liquid, 40 ml of acetone was added yielding a yellow precipitate (748 mg, 32 %). The elemental analysis of the compound agrees well with the calculated values. Anal. calculated: C 19.81, H, 4.95, S 26.41; found: C, 19.90, H 5.04, S 27.11.

2.1.3. Synthesis of [RuCl₂(dip)(DMSO)₂]

Cis-[RuCl₂(DMSO)₄] (286 mg, 0.59 mmol) and 2,7-diphenyl-1,10-phenanthroline (dip) (189 mg, 0.57 mmol) were dissolved in toluene (4 ml). The mixture was heated to reflux under argon for 4 h. The reaction mixture was left overnight at –20 °C. The precipitate was filtered and purified by column chromatography using a silica gel column and acetonitrile as an elution reagent. The solvent was removed later under reduced pressure. The pure product was recrystallized from a mixture of methanol and diethyl ether. Yield: 48 %. Purity was confirmed by HPLC (Fig. S1). [HRMS] (found/calculated) for: [RuCl(dip)(DMSO)]⁺ $m/z = 547.0162/547.0184$; [Ru(dip)(DMSO)₂(OH)]⁺ $m/z = 606.9738/607.0663$; [RuCl(dip)(DMSO)₂]⁺ $m/z = 625.0295/625.0324$.

2.1.4. Synthesis of [Ru(bpy)Cl₂(dip)]

[RuCl₂(dip)(DMSO)₂] (100 mg, 0.15 mmol) and 2,2'-bipyridine (bpy) (22.8 mg, 0.15 mmol) were dissolved in DMF (2 ml). The mixture was heated in a microwave reactor up to 250 °C and immediately cooled. The pure product was obtained after recrystallization from cold acetone, resulting in a 71 % yield (71.15 mg). Purity was confirmed by HPLC (Fig. S1). [HRMS] (found/calculated) for [Ru(bpy)Cl₂(dip)]⁺: $m/z = 660.0428/660.5572$ (Fig. S2).

2.1.5. Synthesis of [Ru(bpy)(dip)(dpq)]Cl₂, [Ru(bpy)(dip)(Me₂dpq)]Cl₂ and [Ru(bpy)(dipb)(dpb)]Cl₂

[Ru(bpy)Cl₂(dip)] (20 mg, 0.030 mmol) and 2,3-bis(2-pyridyl)quinoxaline (dpq) (10 mg, 0.036 mmol), 6,7-dimethyl-2,3-bis(2-pyridyl)quinoxaline (Me_2dpq) (11.4 mg, 0.036 mmol) or 2,3-bis(2-pyridyl)benzo[g]quinoxaline (dipb) (11.7 mg, 0.036 mmol) were dissolved in ethanol (8 ml). The mixtures were refluxed for 4 h under argon. The solvent was then removed under reduced pressure and the resulting solids were dissolved in water (10 ml) and filtrated. The filtrates were dried and dissolved in dichloromethane (1 ml) with a few drops of

methanol. The pure products were precipitated with diethyl ether. [HRMS] (found/calculated): for $[\text{Ru}(\text{bpy})(\text{dip})(\text{dpq})]^{2+}$ ($\text{C}_{52}\text{H}_{36}\text{N}_8\text{Ru}$): $m/z = 437.1011/436.9829$ (22.6 mg, 79 %); for $[\text{Ru}(\text{bpy})(\text{dip})(\text{Me}_2\text{dpq})]^{2+}$ ($\text{C}_{54}\text{H}_{40}\text{N}_8\text{Ru}$): $m/z = 451.1173/451.0095$ (17.4 mg, 60 %); for $[\text{Ru}(\text{bpy})(\text{dip})(\text{dpb})]^{2+}$ ($\text{C}_{56}\text{H}_{38}\text{N}_8\text{Ru}$): $m/z = 462.1066/462.0123$ (23.63 mg, 71 %) (Figs. S3-S5). Despite a clear peak in HRMS analysis, for each Ru(II) complex, the HPLC separation revealed a mixture of isomers designated as fraction A (with a shorter retention time) and fraction B (with a longer retention time) (Fig. 2).

To separate these isomers, preparative thin-layer chromatography (PTLC) was used. Elution was carried out on TLC plates covered with a C18-RP deposit (Macherey-Nagel; Alugram RP-18 W-TLC) using acetonitrile and 0.25 M KNO_3 (3:1) as the mobile phase. After elution, the deposits were scrubbed and complexes were rinsed out with the same eluent and desalted by dissolving and filtering in acetone several times. The solvent was removed under reduced pressure. The resulting solids were dissolved in dichloromethane (1 ml) with a few drops of methanol and precipitated using diethyl ether. HPLC analysis confirmed that the obtained fractions were pure (Fig. 2).

To confirm that the compounds obtained are geometric isomers, ^1H NMR spectra were recorded for all compounds.

$[\text{Ru}(\text{bpy})(\text{dip})(\text{Me}_2\text{dpq})]^{2+}$.

Fraction A: ^1H NMR (600 MHz, MeOD) δ 8.75 (d, $J = 5.5$ Hz, 1H, H-2 or H-9), 8.69 (d, $J = 4.3$ Hz, 1H, H- δ), 8.59 (d, $J = 8.0$ Hz, 1H, H-3' or H-3''), 8.52 (d, $J = 8.0$ Hz, 1H, H-3' or H-3''), 8.39 (q, $J = 9.5$ Hz, 2H, H- α' , H- δ'), 8.35–8.32 (m, 2H, H-5, H-6), 8.26 (d, $J = 5.5$ Hz, 1H, H-2 or H-9), 8.21 (td, $J = 1.6$, 7.7 Hz, 1H, H- α), 8.12–8.07 (m, 2H, H-4', H-4''), 8.05 (d, $J = 14.7$ Hz, 1H, H-6' or H-6''), 7.99 (s, 1H, H-8''), 7.79 (dd, $J = 8.6$, 2.3 Hz, 2H, H-3, H-8), 7.74–7.61 (m, 14H), 7.49 (td, $J = 6.1$, 1.0 Hz, 1H, H-5', H-5''), 7.47 (s, 1H, H-5''), 7.40 (d, $J = 8.3$ Hz, 1H), 7.20 (td, $J = 6.7$, 1.2 Hz, 1H), 2.46 (s, 3H, C-7''– CH_3), 2.08 (s, 3H, C-6''– CH_3).

Fraction B: ^1H NMR (600 MHz, MeOD) δ 8.95 (d, $J = 8.2$ Hz, 1H, H-3' or H-3''), 8.89 (d, $J = 8.1$ Hz, 1H, H- δ), 8.72 (d, $J = 4.6$ Hz, 1H, H-3' or H-3''), 8.68 (d, $J = 5.5$ Hz, 1H, H-2 or H-9), 8.64 (d, $J = 5.5$ Hz, 1H, H-2 or H-9), 8.48 (d, $J = 5.5$ Hz, 1H), 8.33–8.28 (m, 2H, H-4' and H-4''), 8.19 (qd, $J = 4.9$, 1.4 Hz, 2H, H- γ and H- γ'), 8.13 (q, $J = 3.8$ Hz, 2H, H-5 and H-6), 7.97 (d, $J = 5.5$ Hz, 1H, H-3 or H-8), 7.90 (d, $J = 5.5$ Hz, 2H, H-3 or H-8), 7.87 (s, 1H, H-8''), 7.80 (td, $J = 4.4$, 1.6 Hz, 1H), 7.76 (d, $J = 5.3$ Hz, 1H), 7.66–7.60 (m, 6H, H- γ , H- γ' , H- α' , H-3', H-3''), 7.56–7.52 (m, 6H), 7.44 (d, $J = 8.3$ Hz, 1H), 7.41–7.37 (m, 3H, H-5''), 2.36 (s, 3H, C-7''– CH_3), 2.00 (s, 3H, C-6''– CH_3).

$[\text{Ru}(\text{bpy})(\text{dip})(\text{dpq})]^{2+}$.

Fraction A: ^1H NMR (600 MHz, MeOD) δ 8.78 (d, $J = 5.5$ Hz, 1H, H- δ), 8.71 (d, $J = 4.2$ Hz, 1H), 8.53 (d, $J = 8.0$ Hz, 1H, H-3' or H-3''), 8.49 (d, $J = 8.0$ Hz, 1H, H-3' or H-3''), 8.41–8.36 (m, 4H, H- α , H- α'), 8.27–8.21 (m, 3H, H- β , H- β'), 8.08 (tt, $J = 8.0$, 1.4 Hz, 2H, H-4' and H-4''), 7.99 (d, $J = 5.2$ Hz, 1H, H-6' or H-6''), 7.91–7.88 (m, 1H), 7.80–7.78 (m, 2H, H- γ and H- γ'), 7.76–7.61 (m, 16H), 7.53–7.50 (m, 1H), 7.47–7.44 (m, 2H, H-5', H-5''), 7.25–7.22 (m, 1H).

Fraction B: ^1H NMR (600 MHz, MeOD) δ 8.97 (d, $J = 8.2$ Hz, 1H, H- δ), 8.90 (d, $J = 8.0$ Hz, 1H, H-3' or H-3''), 8.75 (d, $J = 4.3$ Hz, 1H, H-6' or H-6''), 8.73 (d, $J = 5.6$ Hz, 1H, H-2 or H-9), 8.59 (d, $J = 5.5$ Hz, 1H, H-2 or H-9), 8.53 (d, $J = 5.0$ Hz, 1H, H- α), 8.39 (d, $J = 7.8$ Hz, 1H, H-3' or H-3''), 8.31 (td, $J = 7.8$, 1.4 Hz, 1H, H- γ), 8.23–8.18 (m, 2H, H-4', H-4''), 8.13 (dd, $J = 8.4$, 1.0 Hz, 1H), 8.10 (d, $J = 3.8$ Hz, 2H, H-5, H-6), 7.93–7.91 (m, 3H, H-3, H-8), 7.85–7.82 (m, 1H), 7.80–7.72 (m, 4H), 7.68–7.66 (m, 2H, H-5', H-5''), 7.62–7.59 (m, 6H), 7.56–7.53 (m, 7H), 7.51 (d, $J = 8.3$ Hz, 1H), 7.45–7.41 (m, 2H), 7.38–7.36 (m, 1H).

$[\text{Ru}(\text{bpy})(\text{dip})(\text{dpb})]^{2+}$.

Fraction A: ^1H NMR (600 MHz, MeOD) δ 8.86 (s, 1H, H-10''), 8.80 (d, $J = 5.5$ Hz, 1H, H-3' or H-3''), 8.72 (d, $J = 4.6$ Hz, 1H, H-3' or H-3''), 8.50 (d, $J = 8.1$ Hz, 1H), 8.44 (t, $J = 6.9$ Hz, 2H, H-5', H-5''), 8.41 (q, $J = 8.4$ Hz, 2H, H-5, H-6), 8.36 (d, $J = 5.5$ Hz, 1H, H- δ), 8.33 (s, 1H, H-5''), 8.31 (d, $J = 5.5$ Hz, 1H, H-2 or H-9), 8.27–8.22 (m, 3H, H-2 or H-9, H-6', H-6''), 8.19 (d, $J = 8.6$ Hz, 1H), 8.11 (t, $J = 7.9$ Hz, 1H), 8.06 (t, $J = 7.9$ Hz, 1H, H-4' or H-4''), 7.83 (d, $J = 5.5$ Hz, 1H, H-3 or H-8), 7.80 (d, $J =$

5.5 Hz, 1H, H-3 or H-8), 7.78–7.70 (m, 8H), 7.69–7.60 (m, 11H), 7.56 (t, $J = 7.6$ Hz, 2H), 7.52–7.50 (m, 2H, H-6'', H-9''), 7.27 (t, $J = 6.6$ Hz, 1H).

Fraction B: ^1H NMR (600 MHz, MeOD) δ 9.00 (d, $J = 8.3$ Hz, 1H, H- δ), 8.95 (d, $J = 8.2$ Hz, 1H, H-3' or H-3''), 8.81 (d, $J = 5.5$ Hz, 1H, H-2 or H-9), 8.75–8.74 (m, 2H, H-6' or H-6'', H-10''), 8.69 (d, $J = 5.5$ Hz, 1H, H-2 or H-9), 8.54 (d, $J = 5.0$ Hz, 1H, H- α), 8.42 (d, $J = 7.7$ Hz, 1H, H-3' or H-3''), 8.31 (td, $J = 8.0$, 1.4 Hz, 1H, H- γ), 8.25 (s, 1H, H-5''), 8.24–8.22 (m, 2H, H-4', H-4''), 8.10 (d, $J = 8.6$ Hz, 1H, H-6'' or H-9''), 8.08 (d, $J = 5.5$ Hz, 1H, H-3 or H-8), 8.03–7.99 (m, 3H), 7.93 (d, $J = 5.5$ Hz, 1H, H-3 or H-8), 7.87–7.84 (m, 1H), 7.83 (d, $J = 5.0$ Hz, 1H), 7.68–7.66 (m, 2H), 7.61–7.59 (m, 5H), 7.55–7.46 (m, 15H), 7.43–7.41 (m, 1H).

2.2. Spectroscopic and physicochemical characterization

The absorption coefficients for the aqueous solutions of the synthesized Ru(II) complexes were measured using a PerkinElmer Lambda 35 spectrophotometer. Stock solutions of the compounds were prepared in DMSO and then dissolved in water. The amount of DMSO in the final solutions did not exceed 5 %. The experiment was repeated three times for each complex. The results are presented as mean values and the standard error of the mean.

The logP values of the studied Ru complexes were determined using the HPLC method, according to a procedure from the literature [28] with some modifications. The isocratic elution of the complexes was performed on an RP-C8 column (Waters) at 25 °C, using a mixture of 0.1 ammonium acetate (water phase) and acetonitrile (organic phase) as a mobile phase. The retention time of the complexes was determined at four different concentrations of organic phase (30–85 %). The retention factor corresponding to the water-only phase ($\log k_w$) was determined from the Snyder-Soczewiński equation: $\log k = \log k_w - S\phi$ (S – slope; ϕ – organic phase content). Ruthenium complexes with known logP values were used as standards [18] ($[\text{Ru}(\text{dip})_3]\text{Cl}_2$, $[\text{Ru}(\text{dip})_2(\text{bpy})]\text{Cl}_2$, $[\text{Ru}(\text{dip})_2(\text{Me}_2\text{bpy})]\text{Cl}_2$ and $[\text{Ru}(\text{bpy})_3]\text{Cl}_2$). LogP of the studied Ru(II) complexes was calculated from the obtained calibration curve.

2.3. Computational characterization

Each of the studied complexes can exist in four different isomeric forms resulting from the possibility of the 2,3-bis(2-pyridyl)quinoxaline and its derivatives to coordinate the metal ion with nitrogen atoms from quinoxaline and/or pyridine fragments. If both quinoxaline and pyridine bind Ru, the five-member ring is formed, whereas two pyridine moieties bind Ru, the seven-member ring is made. Each of these two structural isomers can exist in two conformers, differing by the orientation of the 2,3-bis(2-pyridyl)quinoxaline fragment relative to other ligands. The performed calculations took as starting points all possible structures of complexes.

The ground-state geometries and electronic structures of the Ru(II) complexes were obtained within density functional theory (DFT) using the B3LYP functional and the 6-31G(d, p) basis set for C, N, O, S, H and the LANL2DZ basis set and the effective core potentials for Ru. Electronic excitation spectra were computed within time-dependent density functional theory (TD-DFT) with the same exchange–correlation functional and basis sets. All calculations were done using a polarizable continuum model (PCM), using the integral equation formalism variant (IEFPCM), with ethanol as the solvent. The calculations were obtained in Gaussian 09 program suite [29].

2.4. ROS production in cell-free systems

2.4.1. Fluorescent probes

Fluorescent probes were used to detect ROS production in aqueous solutions in cell-free systems. Fluorescent measurements were made at room temperature using a PerkinElmer LS55 spectrofluorimeter

according to a procedure described elsewhere [26].

Generally, a solution of fluorescent probe and Ru complex (1 μM) in Tris/HCl buffer (0.05 M, pH 7.4) was irradiated with a spectrofluorimeter xenon lamp at the maximum of the metal-to-ligand charge transfer (MLCT) band (**Ru-dpq** – 530 nm, **Ru-Me₂dpq** – 522 nm, **Ru-dpb** – 570 nm). The used light dosage was determined using a Nova II (Ophir) light dosimeter and is indicated in each experiment. After irradiation, the fluorescent spectrum of the probe was measured. Blank measurements without Ru complexes were performed to control the stability of the probe itself during irradiation. Appropriate corrections were made to consider the observed degradation of the probes. The studied Ru complexes were not luminescent, so no correction for their behavior was necessary. Each experiment was repeated at least three times.

The production of singlet oxygen was measured using the Singlet Oxygen Sensor Green probe (SOSG, Thermofisher Scientific, 2.5 μM). The probe was excited at 504 nm and its spectrum was recorded from 504 to 650 nm. Rose bengal was used as a standard for the determination of the quantum yield of $^1\text{O}_2$ [30,31].

The formation of the superoxide anion radical was evaluated using dihydroethidium (HE, AAT Biotechnology). This probe becomes highly fluorescent after reaction with O_2^- and intercalation with DNA. The fluorescence emission spectrum was recorded in the presence of DNA (250 μM) in the range of 550 to 750 nm when excited at 520 nm.

The production of hydroxyl radicals was measured using aminophenyl fluorescein (APF, Enzo, 2.5 μM). This probe was excited at 490 nm, and the spectrum was recorded in the range 500 – 650 nm.

2',7'-dichlorodihydrofluorescein diacetate (**H₂DCF-DA**, Sigma-Aldrich) was used to measure H_2O_2 production. **H₂DCF-DA** is a cellular probe that produces a fluorescent product after reaction with numerous ROS. However, it is particularly sensitive to H_2O_2 , so it can be used to evaluate the H_2O_2 level. **H₂DCF-DA** was initially deacetylated with 0.01 M NaOH to produce 2',7'-dichlorodihydrofluorescein (**H₂DCF**) suitable for use in cell-free systems. This probe was excited at 485 nm and the spectrum was registered in the range 505 – 620 nm. H_2O_2 solutions were used as a reference to convert the measured increase in the fluorescent intensity of DCF into the hydrogen peroxide concentration.

2.4.2. Electron paramagnetic resonance (EPR) spectroscopy

EPR spectroscopy was used to confirm ROS photoproduction by the synthesized Ru(II) complexes in cell-free systems. EPR spectra were recorded at room temperature using an Elexsys E580 CW-EPR spectrometer (Bruker). 100 kHz field modulation along with the 0.2 mT signal modulation amplitude was applied. Parameters for EPR experiment: X band, T = 295 K, microwave power = 0,1 mW, modulation amplitude = 0,1 mT, time constant = 41 ms.

The production of $\cdot\text{OH}$ and O_2^- was verified using a spin trap of 5-dimethyl-1-pyrroline N-oxide (DMPO) [32]. Furthermore, DMPO was used to confirm the generation of H_2O_2 in the presence of Fe^{2+} in the Fenton reaction [33].

Briefly, ruthenium complexes (0.05 μM) were irradiated in the presence of DMPO (35 mM, dissolved in an aqueous solution, pH 4) using a spectrofluorimeter xenon lamp at the maximum of their MLCT band (0.33 mJ/cm^2). After irradiation, EPR spectra were measured to confirm the generation of $\cdot\text{OH}$ or O_2^- .

In separate experiments, Ru(II) complexes (0.5 μM) in Tris/HCl buffer (0.05 M, pH 7.4) were irradiated with a spectrofluorimeter xenon lamp to the maximum of their MLCT band (0.13 mJ/cm^2). After irradiation, the solutions were mixed with DMPO in a 1:1 proportion and FeSO_4 (125 μM) was added. The samples of the resulting solution were sealed in EPR tubes and the spectra were acquired.

Singlet oxygen production was verified using a selective chemical probe 2,2',6,6'-tetramethylpiperidine (TEMP). This spin trap after oxidation produced a stable radical 2,2',6,6'-tetramethylpiperidine-1-oxyl (TEMPO) [34]. The studied Ru(II) complexes (0.05 μM) were added to the TEMP substrate (100 mM, dissolved in Tris/HCl, pH 7.4) and irradiated as previously described (0.33 mJ/cm^2). After that, the

samples were placed in EPR tubes, and EPR measurements were performed.

Spin traps were independently irradiated under identical conditions to avoid false positive results due to trap decomposition after irradiation.

2.5. Cell culture

In vitro studies were conducted using triple negative breast cancer cells MDA-MB-231. Cells were cultured in L-15 medium supplemented with 2 mM glutamine, 15 % fetal bovine serum (FBS) (v/v), and 1 % penicillin–streptomycin solution (100 units/ml–100 $\mu\text{g}/\text{ml}$) (v/v) at 37 °C in a humidified atmosphere and passed 2–3 times a week according to standard aseptic procedures.

2.6. Cytotoxicity and photocytotoxicity

Cell viability upon treatment with Ru(II) complexes was determined using the resazurin assay. Cells were seeded in 96-well plates with a density of 3×10^4 cells per cm^2 in complete medium and cultured for 24 h. Then, the medium was removed, and various concentrations of Ru(II) complexes in the basic medium were added to the wells. Stock solutions of the Ru(II) complexes were prepared in DMSO. The final concentration of DMSO was fixed (0.1 % (v/v)). After 24 h of incubation, cells were washed with PBS and sodium salt of resazurin (50 μM) dissolved in Dulbecco's phosphate buffered saline with Ca^{2+} and Mg^{2+} (DPBS) was added and incubated for 3 h. The amount of fluorescent resorufin was quantified at 605 nm (560 nm excitation light) using a Tecan Infinite 200 microplate reader. The experiments were carried out in triplicate and repeated three times. The results are presented as mean values and the standard error of the mean. The $\text{IC}_{50}^{\text{dark}}$ parameters were determined using the Hill equation (OriginPro 2020).

$$y = y_0 + \frac{(y_{100} - y_0)[c]^H}{[\text{IC}_{50}]^H + [c]^H}$$

The cytotoxicity of the free ligands (**dpq**, **dpb**, **Me₂dpq**) as well as Ru complexes' precursor ([Ru(bpy)Cl₂(dip)]) was evaluated using the same protocol. The concentration range was chosen due to the compounds solubility.

For photocytotoxic studies, MDA-MB-231 cells after incubation with Ru(II) complexes were washed with DPBS and irradiated with monochromatic blue 465 nm light for 10 min (8.6 J/cm^2). After the irradiation, cells were kept in the complete fresh medium for 24 h. The viability assay was then performed and the IC_{50}^{465} values were calculated.

2.7. Ruthenium accumulation in vitro

MDA-MB-231 cells were seeded in 6-well plates with a density of 4×10^4 cells per cm^2 in a complete medium and cultured for 24 h. Subsequently, cells were incubated with 1 μM solution of the complexes in the basic medium for 1, 4, or 24 h. The incubated cells were then washed, detached by trypsin treatment, counted, and centrifuged. Cells were digested in concentrated nitric acid overnight at room temperature. The solutions were then diluted with Millipore water to a final nitric acid concentration of 1 %. Samples were analyzed using inductively coupled plasma mass spectrometry (ICP-MS, NexION 2000, Perkin-Elmer). The results were calculated as the Ru concentration per cell (the cell volume was used as 1700 fl). The experiments were repeated three times.

2.8. ROS production in vitro

MDA-MB-231 cells were seeded in 96-well plates with a density of 3×10^4 cells per cm^2 in complete medium and cultured for 24 h. The medium was removed, and various concentrations of the studied complexes were added for 24 h of incubation. After treatment, cells were

washed with DPBS and fluorescent probes were added to the cell culture ($\text{H}_2\text{DCF-DA}$ (20 μM), SOSG (5 μM), APF (5 μM), and HE (10 μM)) for 30 min of incubation. The probes were then removed, and the cells were washed with DPBS. The fluorescent intensity of the cells was quantified using a Tecan Infinite 200 plate reader using the following excitation/emission wavelengths: 485/535 nm for $\text{H}_2\text{DCF-DA}$, APF, and SOSG and 520/605 nm for HE.

For photo-induced ROS generation cells, after incubation with Ru(II) complexes, MDA-MB-231 cells were washed with DPBS and irradiated with monochromatic blue 465 nm light (8.6 J/cm^2). After that, fluorescent ROS probes were added, and the procedure applied was identical to that carried out in the dark. The experiments were carried out in triplicate and repeated three times to obtain mean values and standard deviation of the mean.

2.9. Trypsin and photo-trypsin resistance assay

MDA-MB-231 cells were seeded in 96-well plates with a density of 3×10^4 cells per cm^2 in complete medium and cultured for 24 h. The complete medium was then removed and various concentrations of the complexes studied were added to the wells for 24 h of incubation. Subsequently, the cells were washed and 30 μl of trypsin solution (0.01 %) was added to each well and incubated for 5 min at 37 $^\circ\text{C}$. The cells were then washed with PBS and a resazurin assay was performed to quantify adherent cells.

For determinations of phototrypsin resistance, cells, after incubation with Ru(II) complexes were washed with DPBS and irradiated with monochromatic blue 465 nm light (8.6 J/cm^2). After irradiation, cells were kept in complete fresh medium for 24 h. Subsequently, the procedure was the same as for the experiment without irradiation.

The results obtained were normalized to the corresponding wells without trypsin treatment to exclude the possible toxicity of the studied

compounds. Results are presented as a percentage of untreated cells. The experiments were carried out in triplicate and each experiment was repeated five times to obtain mean values and standard error of the mean.

3. Results and discussion

3.1. Synthesis and characterization

Fig. 1 shows the pathway for the synthesis of the investigated tris-heteroleptic Ru(II) complexes. As suggested in the literature [19], $[\text{RuCl}_2(\text{DMSO})_4]$ was used as the starting substrate for the synthesis of tris-heteroleptic Ru(II) complexes. $[\text{RuCl}_2(\text{dip})(\text{DMSO})_2]$ was synthesized with the use of low reactive, nonpolar toluene as a solvent and high sufficient substrate concentration of substrates (~120 mg/ml). Such conditions provided a high yield (48 %) of the desired product. The introduction of a second ligand is more effective in a solvent with a high boiling point [19]. The use of microwave-assisted synthesis for this type of complexes has an additional beneficial effect, as it allows the amount of solvent to be reduced and the reaction time to be decreased [35]. Therefore, the second step of synthesis (2,2-bipyridine (**bpy**) introduction) was performed using DMF as a solvent. The reaction was carried out at 250 $^\circ\text{C}$ and with the help of microwave irradiation it took around 3 min. Such conditions, together with an appropriate concentration of substrates (~60 mg/ml), resulted in a yield of 71 % and a lack of side products. The last step, the introduction of 6,7-dimethyl-2,3-bis(2-pyridyl)quinoxaline (**Me₂dpq**), 2,3-bis(2-pyridyl)quinoxaline (**dpq**) or 2,3-bis(2-pyridyl)benzo[*g*]quinoxaline (**dpb**), was performed according to procedures described previously [36]. Low substrate concentrations are crucial during this step to avoid the possible polymerization of Ru complexes. The identity and purity of each step were confirmed by HPLC (Figs. 2 and S1) and HRMS (Figs. S2-S5) analysis.

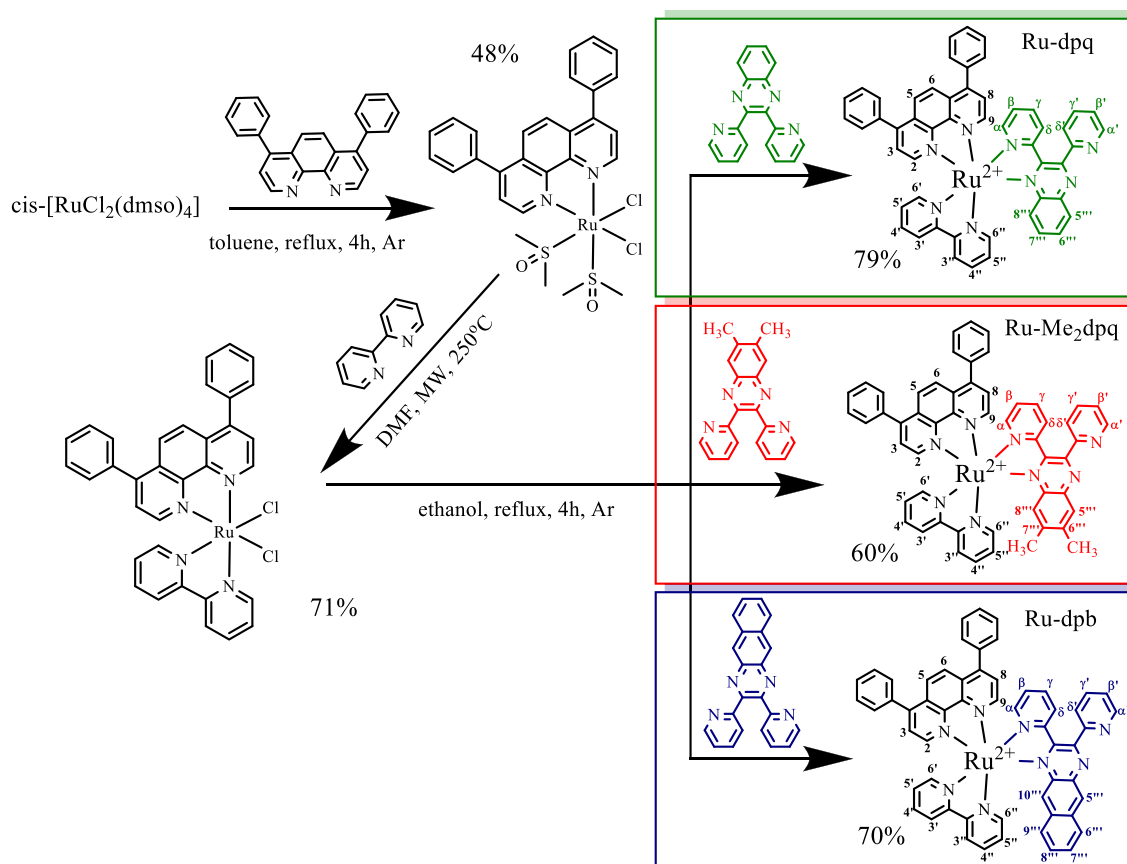


Fig. 1. Synthetic route for $[\text{Ru}(\text{bpy})(\text{dip})\text{L}]^{2+}$.

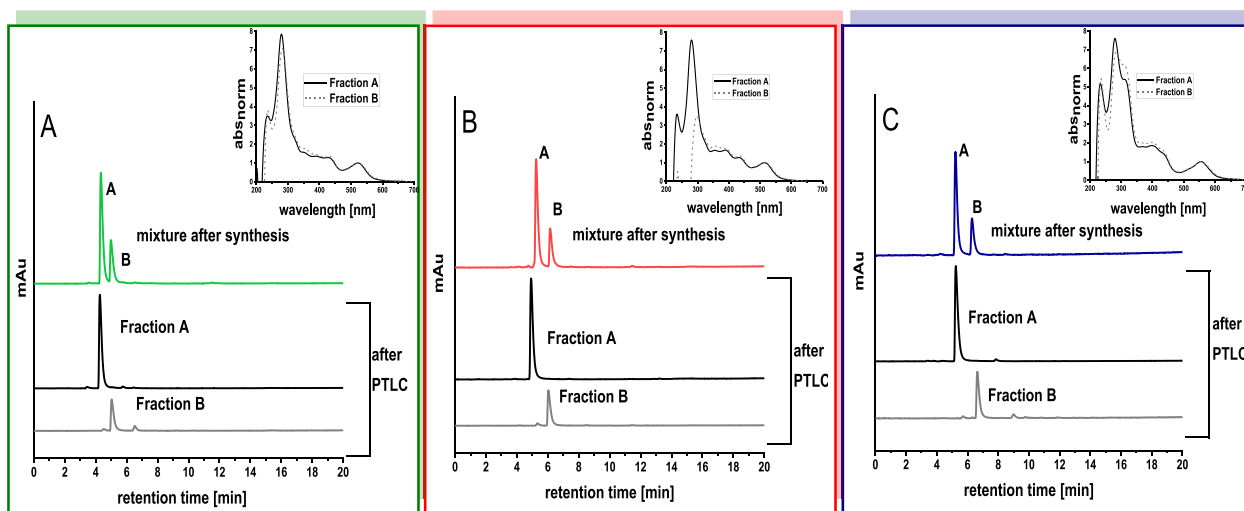


Fig. 2. Chromatograms and UV-vis spectra for each peak of **Ru-dpq** (A), **Ru-Me₂dpq** (B), and **Ru-dpb** (C).

HPLC analysis of the synthesized Ru(II) complexes revealed the presence of two peaks on the chromatograms with slightly different retention times but very similar absorption spectra (Fig. 2). The presence of an unsymmetrical ligand (**dpq**, **dpb**, or **Me₂dpq**) provides two possible coordination geometries to the Ru core: five- or seven-membered chelates. Additionally, as has been shown before [37], three different bidentate ligands in the octahedral structure of Ru complexes can result in different geometric isomers. Therefore, several possible structures of the synthesized complexes need to be considered. Despite our efforts, the growth of suitable crystals of the synthesized Ru complexes was unsuccessful, and thus no single-crystal XRD-based structure of the complexes could be obtained. We focus on quantum chemical calculations within the DFT approach, as well as ¹H NMR spectra analysis for the structural determination of the newly synthesized compounds.

The preparative thin-layer chromatography (PTLC) was used to separate the observed isomers of Ru(II) complexes. The two fractions

obtained were subjected to HPLC analysis and compared with the chromatograms of the mixtures before PTLC separation (Fig. 2). HPLC analysis confirmed that PTLC allowed for the effective separation of isomers. For each of the synthesized complexes, the ratio between isomer A and isomer B was ca. 7:3 (Table S1).

The structures of **Ru-Me₂dpq** isomers A and B were analyzed by ¹H NMR spectroscopy. ¹H NMR spectra of both Ru isomers have shown, that after coordination of **Me₂dpq** ligand to the metallic center, the symmetry of ligand is disturbed. As a result, on the spectra of the complexes, two singlets from protons in CH₃ groups (for **Ru-Me₂dpqA** at 2.46 and 2.08 ppm and **Ru-Me₂dpqB** at 2.36 and 2.00 ppm) were observed (Fig. S6, and 3). Moreover, protons in positions 5'' and 8'' of the quinoxaline ring were correlated with two singlet signals on ¹H NMR spectra (7.99 and 7.47 ppm for isomer A and 7.87 and 7.39 (superimpose with multiplet) for isomer B). Those observations allowed us to conclude that in both complexes the coordination occurs with the formation of a 5-membered “ring” and not via the formation of a 7-

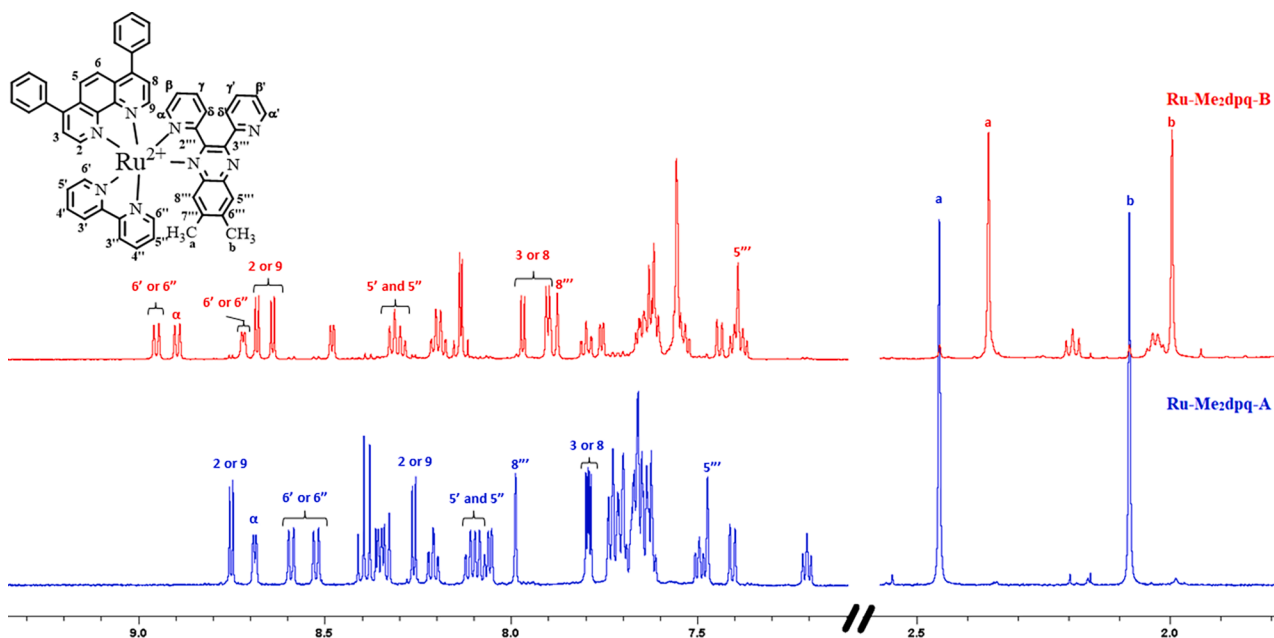


Fig. 3. Comparison of ¹H NMR spectra of **Ru-Me₂dpq** isomers (blue (bottom) - **Ru-Me₂dpqA**, red (top) - **Ru-Me₂dpqB**) with assigned signals for key protons. ((Colour online.))

membered “ring”. The ^1H NMR spectra of **Ru-dpq** and **Ru-dpb** (isomers A and B) gave the similar conclusions (Fig. S7 and S8).

Comparison of ^1H NMR spectra for **Ru-Me₂dpq-A** and **Ru-Me₂dpq-B** were presented in Fig. 3. Both spectra exhibit significant differences in chemical shifts of several protons. In isomer A, pyridine of the 6,7-dimethyl-2,3-bis(2-pyridyl)quinoxaline ligand points towards dip ligand. This cause that signals from dip ligand protons (especially proton 2 and 9) are much further apart and have their signals at 8.26 ppm and 8.75 ppm whereas in isomer B, where pyridine points towards bpy ligand, those signals are close together – at 8.64 ppm and 8.68 ppm. On the contrary, for protons of bpy ligand (3' and 3'') distance between those signals is small 8.52 ppm and 8.59 ppm for isomer A, and much higher for isomer B – 8.72 ppm and 8.95 ppm.

The geometry structures of the studied complexes were proposed by DFT calculations. The complexes with five-membered “ring” are formed when both quinoxaline and pyridine bind Ru, while the complexes with seven-membered “ring” are formed when two pyridine moieties bind Ru. Each of these two structural isomers can exist in two conformers. The geometry structures of all isomers were optimized (see Fig. S9 for **Ru-dpq** isomers), and the energy differences between all isomers are listed in Table S2 in the Supplementary Information file supplemented by the bond lengths of the key bonds. The computed free Gibbs energies indicate that Ru(II) complexes with the five-membered “ring” geometries are more stable than those with the seven-membered “rings” (the differences are ca. 11 kcal/mol for each of the complexes). This finding agrees with the structural data provided by ^1H NMR spectroscopy as well as with data from the literature [26,38–41]. Isomers A differ from isomers B by the orientation of the 2,3-bis(2-pyridyl)quinoxaline fragment: in the A isomer pyridine points toward the **dip** ligand, while in the B isomer pyridine points towards the **bpy** one. The computed free Gibbs energies indicate that the isomer A is more stable, which is reflected in its preferred formation compared to the isomer B.

Since isomers A were produced with significantly higher efficiency (Table S1), those isomers were chosen for further spectroscopic, physicochemical, and biological analysis. The UV–vis absorption spectra of the metal complexes as well as complexes’s precursor (Ru(bpy)(dip)Cl₂) and free ligands are shown in Fig. 4 and S10. The absorption coefficients of synthesized Ru complexes at various wavelengths are provided in Table 1. The stability of the Ru(II) compounds in an aqueous solution up to 24 h of incubation was confirmed by UV–vis spectroscopy.

In the UV region of the complexes spectra, the intense and sharp bands correspond to a spin allowed intra-ligand (IL) transition [18]. The high-intensity absorption band around 400 nm can be attributed mainly

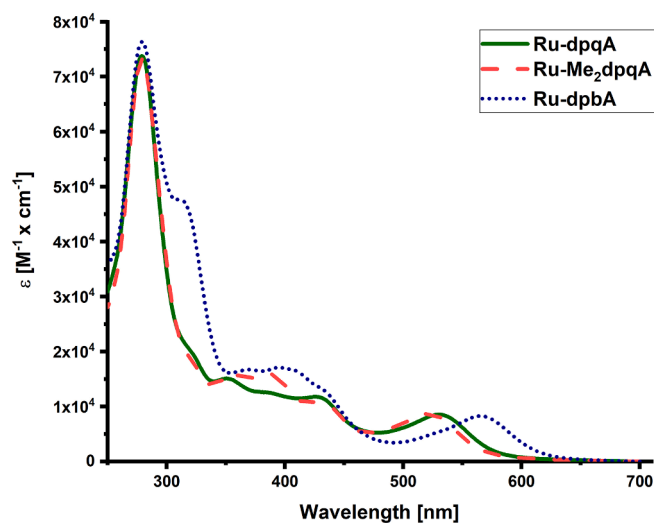


Fig. 4. UV–vis absorption spectra of Ru(II) polypyridyl compounds in aqueous solution (H₂O, DMSO < 5 %, RT).

Table 1

Molar absorption coefficients (in water) and logP parameters of the studied Ru (II) compounds.

Ru complex	$\lambda_1(\epsilon)$ [$\text{nm}(\epsilon \times 10^4 \text{ M}^{-1} \text{ cm}^{-1})$]	$\lambda_2(\epsilon)$ [$\text{nm}(\epsilon \times 10^4 \text{ M}^{-1} \text{ cm}^{-1})$]	LogP
Ru-dpqA	351 (1.54 ± 0.04)	530 (0.87 ± 0.02)	-0.09 ± 0.06
Ru-Me₂dpqA	357 (1.55 ± 0.05)	522 (0.85 ± 0.03)	0.11 ± 0.06
Ru-dpbA	394 (1.57 ± 0.1)	565 (0.76 ± 0.05)	0.22 ± 0.07

to an intra-ligand charge transfer (ILCT), although some MLCT contribution should be considered [42,43]. With respect to free ligand, the IL/ILCT bands are red shifted by around 50 nm, because the energy of the LUMO localized on dpq ligand is lowered upon coordination to ruthenium(II) [44]. The absorption in the visible region around 530 nm is assigned to a MLCT transition as observed in ruthenium polypyridyl complexes [18,45,46]. Modification of the dpq ligand with an additional phenyl ring increases the delocalized π -electron system, by this reduces the energy of the metal-to-ligand charge transfer (MLCT), which results in a shift of the absorption band towards longer wavelengths [47]. The absorption MLCT band in the visible region of the spectrum for **Ru-dpqA** had a maximum at 530 nm, while for **Ru-dpbA** it occurred at 565 nm. Such an increase in the wavelength of the MLCT transition is a desirable effect in the case of potential applications of Ru complexes in PDT. The introduction of methyl groups into the dpq ligand resulted in a small hypsochromic shift in the maximum MLCT at 522 nm for **Ru-Me₂dpqA**. The studied complexes were not luminescent upon excitation at the MLCT band.

DFT calculations allowed the characterization of the frontier orbitals of the complexes (see Fig. S11). HOMOs are made up mainly of Ru d orbitals with an admixture of 2,3-bis(2-pyridyl)quinoxaline fragments (dpq, Me₂dpq and dpb). LUMOs are mainly composed of 2,3-bis(2-pyridyl)quinoxaline fragments with a smaller contribution of Ru d orbitals. TD-DFT calculations allowed us also to conclude that the main absorption bands of the studied complexes are of the MLCT character.

The lipophilicity of the newly synthesized complexes was determined using the HPLC method [28], adapted for Ru complexes. The determined logP values for Ru compounds are presented in Table 1. As can be seen, modification of the dpq ligand either with methyl substituents or with a phenyl ring increases the logP value of the complexes. Furthermore, the difference between the elution time of isomer A and isomer B of the compounds was observed to depend directly on the lipophilicity of the complex. Higher logP values correlate with a greater difference between the retention times of individual isomers (Table S1).

3.2. Reactive oxygen species production in aqueous systems

The efficiency of ROS production by synthesized Ru(II) complexes under cell-free conditions was assessed using a variety of fluorescent probes and EPR spin traps. These values can be used to evaluate the potential of these compounds to serve as effective photosensitizers.

The generation of $^1\text{O}_2$ in aqueous solution by irradiation of the synthesized Ru complexes in the MLCT bands was detected qualitatively by EPR spectroscopy (Fig. 5A). Upon oxidation with singlet oxygen, the TEMP substrate was converted to the paramagnetic product TEMPO, the spectrum of which was easily measured by EPR spectroscopy [34]. The quantum yield of $^1\text{O}_2$ production was measured using the singlet oxygen sensor green (SOSG) probe. In air-saturated Tris/HCl buffer (pH 7.4) Φ_Δ was 0.3 – 0.7 for all studied complexes. Modification of the dpq ligand successfully decreased the efficiency of $^1\text{O}_2$ generation. The addition of a phenyl ring to this ligand caused a reduction of Φ_Δ to one-third of its initial value. It should be taken into account that the Φ_Δ values obtained can be slightly overestimated since the SOSG probe itself can serve as a singlet oxygen photosensitizer [48].

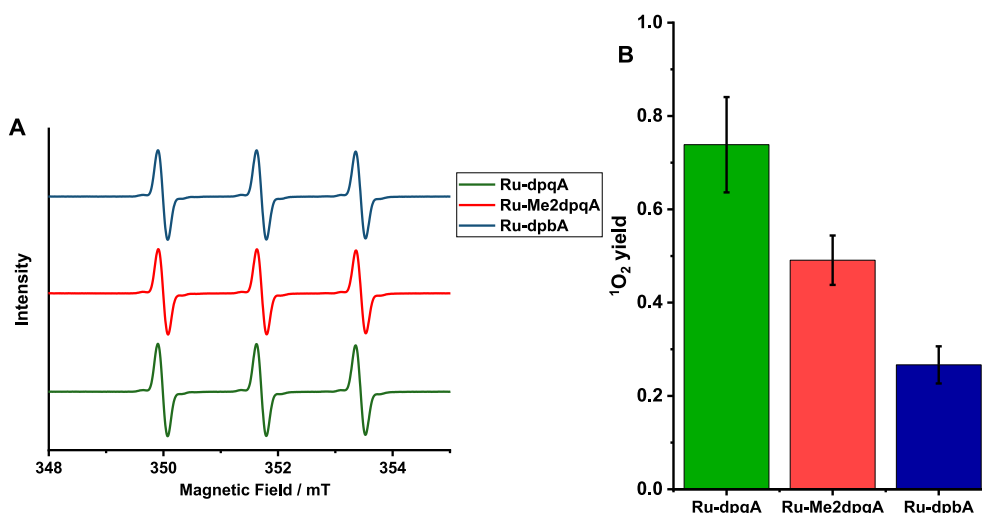


Fig. 5. (A) EPR spectra of TEMP oxidation to TEMPO upon irradiation of 0.05 μM Ru-dpqA, Ru-Me₂dpqA, and Ru-dpbA at 530, 522, or 565 nm, respectively, light dose 3.3×10^{-4} J/cm². 0.05 M Tris/HCl buffer, pH 7.4, RT. (B) Photogeneration of ¹O₂ (Φ_{Δ}) by Ru complexes upon their irradiation at MLCT bands.

The phototoxicity of Ru(II) polypyridyl complexes depends not only on their singlet oxygen generation [22], therefore the production of other types of ROS was evaluated. The superoxide anion radical O₂^{•-} can be detected using either EPR (by applying the DMPO spin trap) or fluorescence spectroscopy (by the used of dihydroethidium (HE) probe). The lack of noticeable changes in EPR or fluorescent spectra indicated that the heteroleptic Ru(II) complexes did not produce O₂^{•-} upon irradiation. The generation of hydroxyl radicals can be followed using EPR (DMPO) or fluorescent (aminophenyl fluorescein, APF) probes. Upon irradiation of Ru(II) complexes, no changes in APF spectra were observed. However, the irradiation of Ru complexes with DMPO spin trap revealed the characteristic spectrum of the DMPO-OH adduct (Fig. S12) that confirms the minor production of •OH.

The production of H₂O₂ was monitored using 2',7'-dichlorodihydrofluorescein (H₂DCF). All studied Ru(II) complexes upon irradiation induced a significant increase in the fluorescence of this probe. Recalculation of the DCF fluorescent signal in H₂O₂ concentration revealed that 1 μM Ru compounds can produce from 200 to 500 μM of hydrogen peroxide (Fig. 6A). The calculated values could be slightly overestimated since H₂DCF is reactive to various ROS [49], however, it is the most sensitive to H₂O₂. The production of H₂O₂ was confirmed by EPR spectroscopy (Fig. 6B). The amount of the photogenerated H₂O₂, which was detected upon irradiation of heteroleptic Ru(II) complexes is significantly higher, than for homoleptic ones [26].

3.3. Cytotoxicity and photocytotoxicity toward breast cancer cells

The cytotoxicity and photocytotoxicity of the Ru complexes studied were assessed against the highly invasive triple-negative breast cancer cell line MDA-MB-231. The cytotoxicity of compounds in the dark (IC₅₀^{dark}) varies from 4 μM (for Ru-dpbA) to 63 μM (for Ru-dpqA) (Table 2) All compounds were found to be more cytotoxic than cisplatin (IC₅₀ = 83 μM), used as a reference (results are not shown). Free ligands and Ru complexes' precursor were found to be non-toxic in the studied concentration range (0–32 μM), so cytotoxicity of polypyridyl Ru(II) complexes originated from their tris-heteroleptic structures. Cytotoxicity of the compounds correlated well with their time-dependent accumulation, measured by the ICP-MS technique (Fig. S13). On the other hand, these parameters depend on the lipophilicity of the compounds (logP values, Table 1). Such a correlation was expected and has been previously reported by us and others [26,50,51].

Table 2

Cytotoxicity (IC₅₀^{dark}) and photocytotoxicity (IC₅₀⁴⁶⁵) values, as well as photo-therapeutic index (PI = IC₅₀^{dark}/IC₅₀⁴⁶⁵) values for the studied Ru complexes determined against the MDA-MB-231 cell line after 24 h of incubation.

Ru complex	IC ₅₀ ^{dark} / μM	IC ₅₀ ⁴⁶⁵ / μM	PI
Ru-dpqA	65.0 ± 4.5	2.1 ± 0.3	30.95
Ru-Me ₂ dpqA	19.9 ± 1.1	3.4 ± 0.3	5.85
Ru-dpbA	4.2 ± 1.1	0.6 ± 0.1	7.00

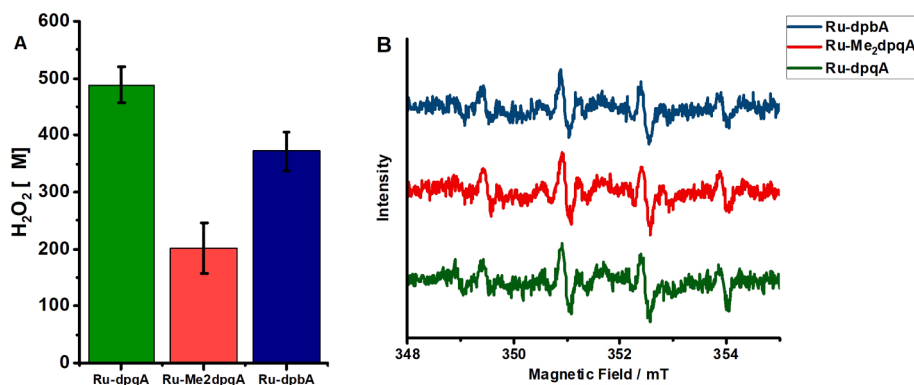


Fig. 6. (A) The amount of H₂O₂ generated after irradiation of 1 μM Ru-dpqA, Ru-Me₂dpqA, and Ru-dpbA at 530, 522, or 565 nm, respectively. Light dose 2.7×10^{-4} J/cm². (B) DMPO EPR spectra after irradiation of Ru complexes (0.5 μM , 1.3×10^{-4} J/cm²) in the presence of Fe²⁺. 0.05 M Tris/HCl buffer, pH 7.4, RT.

The toxicity of the complexes increased dramatically after irradiation. Irradiation of Ru-treated cells with monochromatic blue light (465 nm, 8.6 J/cm²) resulted in a decrease in IC₅₀⁴⁶⁵ values by up to a few μM. The phototherapeutic index (PI), calculated as the ratio of dark to light IC₅₀ values revealed that **Ru-dppqA** was the most phototoxic compound among the studied (PI > 30) (Table 2). It can be partly explained by its low cytotoxicity in the dark. Additionally, **Ru-dppqA** was found to be the best photosensitizer in aqueous solutions, in terms of the formation of ¹O₂ and H₂O₂. High cytotoxicity of the studied Ru(II) complexes can be a serious limitation in their future possible use as PDT agents. This drawback can be reduced by modifying the used concentration of Ru compounds (to achieve photocytotoxicity upon irradiation but not cytotoxicity in the dark) or by applying a specific delivery system (for example selective nanocarriers) to decrease cytotoxicity in the dark.

To better understand the mechanism of phototoxicity induced by the Ru complexes studied, a set of fluorescent probes (SOSG, HE, APF, H₂DCF) was used to detect ROS formation resulting from irradiation of cells exposed to these Ru complexes (Figs. 7, S14). Extremely low concentrations of complexes were added to cells (IC₅₀⁴⁶⁵/8, IC₅₀⁴⁶⁵/4) to limit the ROS assessment to only those produced in cells after irradiation. Such concentrations did not induce ROS production in the MDA-MB-231 cell line in the dark. Irradiation of Ru-treated cells resulted in the production of high amounts of H₂O₂ (Fig. 7A). The generation of singlet oxygen was also measured (Fig. 7B). Apart from ¹O₂ and H₂O₂, no other reactive oxygen species were detected (Fig. S14). **Ru-dppqA** was once again identified as the most efficient ROS-producing complex *in vitro*.

3.4. Influence on cancer cell adhesion properties

It has recently been shown that in addition to their cytotoxic and phototoxic activity, Ru(II) polypyridyl complexes can alter the adhesion properties of various cancer cells [51–56]. Light activation can further modulate the antimetastatic activity of Ru compounds [24].

The trypsin resistance assay, described in detail in our recent review [57], was used to evaluate the influence of the synthesized Ru complexes on the adhesion properties of MDA-MB-231 cells. To exclude the toxicity of the complexes, low nontoxic concentrations (IC₅₀/4, IC₅₀/8) were used for an evaluation. The tested Ru(II) complexes significantly decreased the susceptibility of MDA-MB-231 cells to trypsin detachment (Fig. 8A). The strongest effect was observed for **Ru-dpbA**, which correlates with the accumulation and lipophilicity of the compound. To check whether changes in the adhesion properties of cancer cells induced by the studied Ru(II) complexes can be further modulated with the use of irradiation, we also performed a trypsin resistance assay on irradiated Ru-treated cells. The concentrations used for the complexes were appropriately decreased (to IC₅₀^{dark}/4 and IC₅₀^{dark}/8) to avoid

photocytotoxicity of the compounds. Such small concentrations did not induce changes in the adhesion properties of MDA-MB-231 cells in the dark (results are not shown). However, the irradiation of Ru-treated cells with monochromatic 465 nm light significantly increased the number of tumor cells that were resistant to trypsin treatment (Fig. 8B). Therefore, even very small, non-photocytotoxic concentrations of the synthesized Ru(II) complexes upon light activation changed the adhesion properties of cancer cells.

4. Conclusions

Three novel heteroleptic Ru(II) polypyridyl complexes were synthesized with the assistance of microwave irradiation. The obtained mixture of isomers was successfully separated by PTLC. DFT calculations indicated that in the synthesized complexes, Ru atoms form five-membered “rings” with ligands based on 2,3-bis(2-pyridyl)quinoxaline. They can co-exist in two isomeric forms, out of which the one with pyridine pointing toward the **dip** ligand is more stable. ¹H NMR spectroscopy confirmed the findings of the DFT calculations. The described synthetic procedures can be applied to prepare different tris-heteroleptic Ru(II) polypyridyl compounds. This will increase the accessibility to a larger variety of Ru structures, which in turn will lead to the more efficient selection of complexes with the desired properties.

The synthesized Ru complexes were investigated for their potential application as PDT agents. All complexes studied exhibited significant photocytotoxic activity under irradiation with a low dose of monochromatic visible light. However, the compounds were found to be cytotoxic in the dark, which can limit their application in PDT. **Ru-dppqA** has the greatest potential as PDT agent as the least cytotoxic compound in the dark with phototherapeutic index PI > 30. Their photodynamic activity was based on both type-I and type-II sensitized oxidation mechanisms, as confirmed by studies in cellular systems and by solution-based studies. Such dual reactivity can be beneficial for PDT activity in cells under decreased oxygen conditions. **Ru-dppqA** was found to be the most promising photodynamic agent among the compounds studied due to both low cytotoxicity in the dark and high efficiency of H₂O₂ and ¹O₂ generation. Furthermore, the study on the antimetastatic activity of Ru complexes revealed that nontoxic concentrations of the complexes strengthened the adhesion properties of cancer cells. Irradiation further enhanced this activity and allowed a significant influence on the adhesion of cancer cells at much lower concentrations of Ru complexes. This finding unravels an additional benefit of Ru(II) polypyridyl complexes as PDT agents.

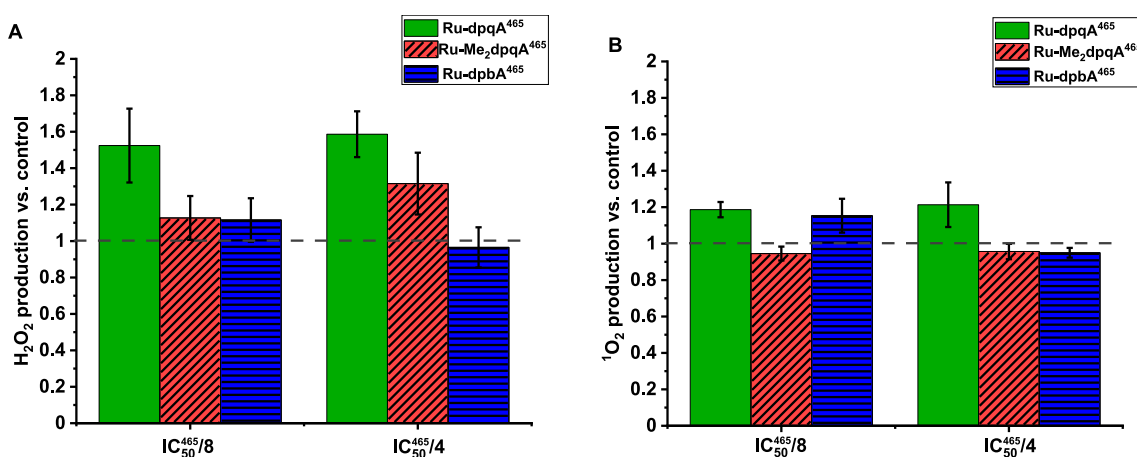


Fig. 7. ROS formation upon treatment of MDA-MB-231 cells with nontoxic concentrations of Ru(II) complexes upon irradiation with 465 nm light (8.6 J/cm²). The formation of H₂O₂ was evaluated with the H₂DCF-DA probe (A), while the generation of ¹O₂ was measured with the SOSG probe (B).

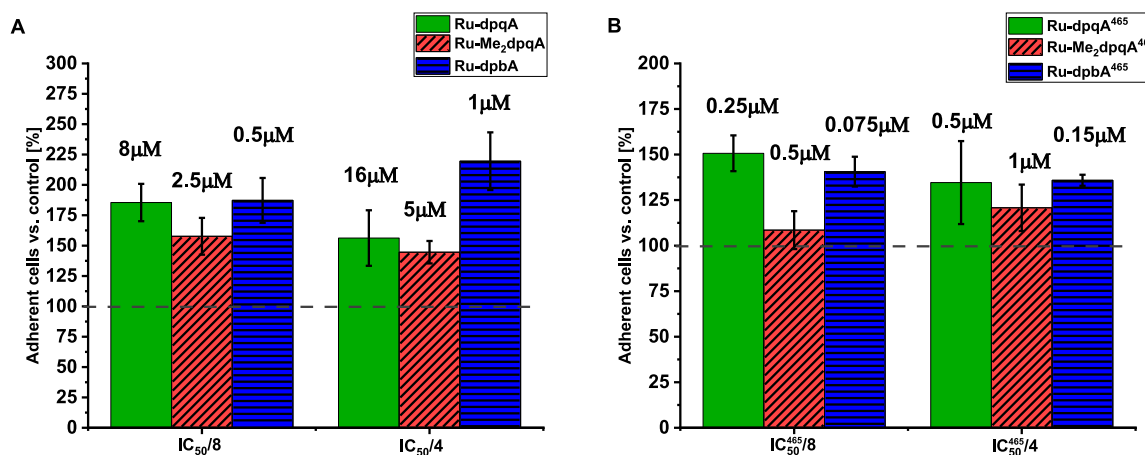


Fig. 8. The change in the adhesion properties of MDA-MB-231 cells was evaluated as the percentage of remaining adherent cells after controlled trypsin treatment. Cells were treated for 24 h with Ru-dpqA, Ru-Me₂dpqA (dashed), and Ru-dpbA (horizontal) without irradiation (A) and after 465 nm light irradiation (8.6 J/cm², B). Untreated cells were used as a control (100 %).

CRedit authorship contribution statement

Ilona Gurgul: Investigation, Writing – original draft. **Olga Mazuryk:** Conceptualization, Investigation, Supervision, Writing – original draft, Writing – review & editing, Funding acquisition. **Dorota Rutkowska-Zbik:** Investigation. **Michał Łomzik:** Investigation. **Aneta Krasowska:** Investigation. **Piotr Pietrzyk:** Writing – review & editing. **Grażyna Stochel:** Writing – review & editing, Funding acquisition. **Małgorzata Brindell:** Conceptualization, Supervision, Writing – review & editing, Funding acquisition.

Declaration of Competing Interest

The authors declare that they have no known competing financial interests or personal relationships that could have appeared to influence the work reported in this paper.

Data availability

Data will be made available on request.

Acknowledgments

O. M. is thankful for the financial support from the National Science Center within the Preludium project (2013/11/N/ST5/01606). M. B. thanks the National Science Center for the financial support (DEC-2016/21/B/NZ7/01081). I. G. acknowledges the support of InterDokMed project no. POWR.03.02.00-00-I013/16. The authors thank Kamil Kubicki for his preliminary work regarding the synthesis of Ru(II) complexes.

Appendix A. Supplementary data

Supplementary data to this article can be found online at <https://doi.org/10.1016/j.poly.2022.116049>.

References

- W. Hua, G. Xu, J. Zhao, Z. Wang, J. Lu, W. Sun, S. Gou, DNA-targeting Ru(II)-polypyridyl complex with a long-lived intraligand excited state as a potential photodynamic therapy agent, *Chem. Eur. J.* 26 (2020) 17495–17503.
- J.P. Celli, B.Q. Spring, I. Rizvi, C.L. Evans, K.S. Samkoe, S. Verma, B.W. Pogue, T. Hasan, Imaging and photodynamic therapy: Mechanisms, monitoring, and optimization, *Chem. Rev.* 110 (2010) 2795–2838.
- M. Mital, Z. Ziara, Biological applications of Ru(II) polypyridyl complexes, *Coord. Chem. Rev.* 375 (2018) 434–458.
- S.J. Steinke, S. Gupta, E.J. Piechota, C.E. Moore, J.J. Kodanko, C. Turro, Photocytotoxicity and photoinduced phosphine ligand exchange in a Ru(II) polypyridyl complex, *Chem. Sci.* 13 (2022) 1933–1945.
- H. Huang, B. Yu, P. Zhang, J. Huang, Y. Chen, G. Gasser, L. Ji, H. Chao, Highly charged ruthenium(II) polypyridyl complexes as lysosome-localized photosensitizers for two-photon photodynamic therapy, *Angew. Chem.* 54 (2015) 14049–14052.
- M. He, F. Du, W.Y. Zhang, Q.Y. Yi, Y.J. Wang, H. Yin, L. Bai, Y.Y. Gu, Y.J. Liu, Photoinduced anticancer effect evaluation of ruthenium(II) polypyridyl complexes toward human lung cancer A549 cells, *Polyhedron* 165 (2019) 97–110.
- P. Sudhindra, S. Ajay Sharma, N. Roy, P. Moharana, P. Paira, Recent advances in cytotoxicity, cellular uptake and mechanism of action of ruthenium metalodrugs: A review, *Polyhedron* 192 (2020) 114827.
- S. Estalayo-Adrián, G.J. McManus, H.L. Dalton, A.J. Savyasachi, J.M. Kelly, T. Gunnlaugsson, Functionalisation of gold nanoparticles with ruthenium(II) polypyridyl complexes for their application in cellular imaging, *Dalton Trans.* 49 (2020) 14158–14168.
- W. Xu, J. Zuo, L. Wang, L. Ji, H. Chao, Dinuclear ruthenium(II) polypyridyl complexes as single and two-photon luminescence cellular imaging probes, *Chem. Comm.* 50 (2014) 2123–2125.
- S. Estalayo-Adrián, S. Blasco, S.A. Bright, G.J. McManus, G. Orellana, D. C. Williams, J.M. Kelly, T. Gunnlaugsson, Effect of alkyl chain length on the photophysical, photochemical, and photobiological properties of ruthenium(II) polypyridyl complexes for their application as DNA-targeting, cellular-imaging, and light-activated therapeutic agents, *ACS Appl. Bio Mater.* 4 (9) (2021) 6664–6681.
- P. Zhang, W. Huang, Y. Wang, H. Li, C. Liang, C. He, H. Wang, Q. Zhang, Isomeric ruthenium(II) complexes for cancer therapy and cellular imaging, *Inorg. Chim. Acta* 469 (2018) 593–599.
- G. Leem, Z.A. Morseth, K.R. Wee, J. Jiang, M.K. Brennaman, J.M. Papanikolas, K. S. Schanze, Polymer-based ruthenium(II) polypyridyl chromophores on TiO₂ for solar energy conversion, *Chem. Asian J.* 11 (2016) 1257–1267.
- M.K. Nazeeruddin, E. Müller, R. Humphry-Baker, N. Vlachopoulos, M. Grätzel, Redox regulation in ruthenium(II) polypyridyl complexes and their application in solar energy conversion, *Dalton Trans.* (23) (1997) 4571–4578.
- S. Monro, K.L. Colón, H. Yin, J. Roque, P. Konda, S. Gujar, R.P. Thummel, L. Lilje, C.G. Cameron, S.A. McFarland, Transition metal complexes and photodynamic therapy from a tumor-centered approach: challenges, opportunities, and highlights from the development of TLD1433, *Chem. Rev.* 119 (2019) 797–828.
- S.A. McFarland, A. Mandel, R. Dumoulin-White, G. Gasser, Metal-based photosensitizers for photodynamic therapy: the future of multimodal oncology? *Curr. Opin. Chem. Biol.* 56 (2020) 23–27.
- S.S. Bhat, A.S. Kumbhar, N. Purandare, A. Khan, G. Grampp, P. Lönnecke, E. Hey-Hawkins, R. Dixit, K. Vanka, Tris-heteroleptic ruthenium(II) polypyridyl complexes: Synthesis, structural characterization, photophysical, electrochemistry and biological properties, *J. Inorg. Biochem.* 203 (2020).
- S. Li, J. Zhao, X. Wang, G. Xu, S. Gou, Q. Zhao, Design of a tris-heteroleptic Ru(II) complex with red-light excitation and remarkably improved photobiological activity, *Inorg. Chem.* 59 (2020) 11193–11204.
- O. Mazuryk, K. Magiera, B. Rys, F. Suzenet, C. Kieda, M. Brindell, Multifaceted interplay between lipophilicity, protein interaction and luminescence parameters of non-intercalative ruthenium(II) polypyridyl complexes controlling cellular imaging and cytotoxic properties, *J. Biol. Inorg. Chem.* 19 (2014) 1305–1316.
- S.M. Zakeeruddin, M.K. Nazeeruddin, R. Humphry-Baker, M. Grätzel, V. Shklover, Stepwise assembly of tris-heteroleptic polypyridyl complexes of ruthenium(II), *Inorg. Chem.* 37 (1998) 5251–5259.
- F.E. Poynton, S.A. Bright, S. Blasco, D.C. Williams, J.M. Kelly, T. Gunnlaugsson, The development of ruthenium(II) polypyridyl complexes and conjugates for: In vitro cellular and in vivo applications, *Chem. Soc. Rev.* 46 (2017) 7706–7756.

- [21] L. Hong, J. Li, Y. Luo, T. Guo, C. Zhang, S. Ou, Y. Long, Z. Hu, Recent advances in strategies for addressing hypoxia in tumor photodynamic therapy, *Biomolecules* 12 (1) (2022) 81.
- [22] Y.Y. Wang, Y.C. Liu, H. Sun, D.S. Guo, Type I photodynamic therapy by organic-inorganic hybrid materials: From strategies to applications, *Coord. Chem. Rev.* 395 (2019) 46–62.
- [23] Z. Lv, H. Wei, Q. Li, X. Su, S. Liu, K.Y. Zhang, W. Lv, Q. Zhao, X. Li, W. Huang, Achieving efficient photodynamic therapy under both normoxia and hypoxia using cyclometalated Ru (II) photosensitizer through type I photochemical process, *Chem. Sci.* 9 (2018) 502–512.
- [24] V. Ramu, S. Aute, N. Taye, R. Guha, M.G. Walker, D. Mogare, A. Parulekar, J. A. Thomas, S. Chattopadhyay, A. Das, Photo-induced cytotoxicity and anti-metastatic activity of ruthenium(II)-polypyridyl complexes functionalized with tyrosine or tryptophan, *Dalton Trans.* 46 (2017) 6634–6644.
- [25] H.A. Goodwin, F. Lions, Tridentate chelate compounds. II, *J. Am. Chem. Soc.* 81 (1959) 6415–6422.
- [26] O. Mazuryk, E. Janczy-Cempa, J. Łagosz, D. Rutkowska-Zbik, A. Machnicka, A. Krasowska, P. Pietrzyk, G. Stochel, M. Brindell, Relevance of the electron transfer pathway in photodynamic activity of Ru(II) polypyridyl complexes containing 4,7-diphenyl-1,10-phenanthroline ligands under normoxic and hypoxic conditions, *Dalton Trans.* 51 (2022) 1888–1900.
- [27] T. Bora, M.M. Singh, Sulphoxide complexes of ruthenium, *Trans. Met. Chem.* 3 (1) (1978) 27–31.
- [28] D.J. Minick, J.H. Frenz, M.A. Patrick, D.A. Brent, A comprehensive method for determining hydrophobicity constants by reversed-phase high-performance liquid chromatography, *J. Med. Chem.* 31 (10) (1988) 1923–1933.
- [29] M. J. Frisch, G.W. Truck, H. B. Schlegel, G. E. Scuseria, M. A. Robb, J. R. Cheeseman, G. Scalmani, V. Barone, G. A. Petersson, H. Nakatsuji, M.C. X. Li, A. Marenich, J. Bloino, B. G. Janesko, R. Gomperts, B. Mennucci, H. P. Hratchian, J. V. Ortiz, A. F. Izmaylov, J. L. Sonnenberg, D. Williams-Young, F.L. F. Ding, F. Egidi, J. Goings, B. Peng, A. Petrone, T. Henderson, D. Ranasinghe, V. G. Zakrzewski, J. Gao, N. Rega, G. Zheng, W. Liang, M. Hada, M. Ehara, K. Toyota, R. Fukuda, J. Hasegawa, M. Ishida, T. Nakajima, Y. Honda, O. Kitao, H. Nakai, T. Revren, K. Throssell, J. A. Montgomery, J.E.P. Jr., F. Ogliaro, M. Bearpark, J. J. Heyd, E. Brothers, K. N. Kudin, V. N. Staroverov, T. Keith, R. Kobayashi, J. Normand, K. Raghavachari, A. Rendell, J. C. Burant, S. S. Iyengar, J. Tomasi, M. Cossi, J. M. Millam, M. Klene, C. Adamo, R. Cammi, J. W. Ochterski, R. L. Martin, K. Morokuma, O. Farkas, J. B. Foresman, D. J. Fox, , 2016., Gaussian, Inc., in, Wallingford CT, 2016.
- [30] J.J.M. Lamberts, D.C. Neckers, Rose Bengal derivatives as singlet oxygen sensitizers, *Tetrahedron* 41 (11) (1985) 2183–2190.
- [31] I.E. Kochevar, R.W. Redmond, Photosensitized production of singlet oxygen, *Methods Enzymol.* (2000) 20–28.
- [32] K.K. Griendling, R.M. Touyz, J.L. Zweier, S. Dikalov, W. Chilian, Y.R. Chen, D. G. Harrison, A. Bhatnagar, Measurement of reactive oxygen species, reactive nitrogen species, and redox-dependent signaling in the cardiovascular system: a scientific statement from the American Heart Association, *Circ. Res.* 119 (2016) e39–e75.
- [33] M.S. Jeong, K.-N. Yu, H.H. Chung, S.J. Park, A.Y. Lee, M.R. Song, M.-H. Cho, J. S. Kim, Methodological considerations of electron spin resonance spin trapping techniques for measuring reactive oxygen species generated from metal oxide nanomaterials, *Sci. Rep.* 6 (1) (2016).
- [34] C.E. Díaz-Urbe, W.A. Vallejo-Lozada, F. Martínez-Ortega, Photooxidation of anthracene under visible light with metalcarboxyphenylporphyrins, *Rev. Fac. Ing.* 1 (2014) 225–230.
- [35] J. Cao, Q. Wu, W. Zheng, L. Li, W. Mei, Microwave-assisted synthesis of polypyridyl ruthenium(II) complexes as potential tumor-targeting inhibitors against the migration and invasion of Hela cells through G2/M phase arrest, *RSC Adv.* 7 (2017) 26625–26632.
- [36] M. Łomzik, O. Mazuryk, D. Rutkowska-Zbik, G. Stochel, P.C. Gros, M. Brindell, New ruthenium compounds bearing semicarbazone 2-formylpyridine moiety: Playing with auxiliary ligands for tuning the mechanism of biological activity, *J. Inorg. Biochem.* 175 (2017) 80–91.
- [37] O. Johansson, Ruthenium(II) polypyridyl complexes: applications in artificial photosynthesis, in: *Stockholm: Institutionen för organisk kemi*, 2004, pp. 60.
- [38] Y. Chen, W. Lei, G. Jiang, Y. Hou, C. Li, B. Zhang, Q. Zhou, X. Wang, Fusion of photodynamic therapy and photoactivated chemotherapy: A novel Ru(II) arene complex with dual activities of photobinding and photocleavage toward DNA, *Dalton Trans.* 43 (2014) 15375–15384.
- [39] A.A. Abdel-Shafi, M.M.H. Khalil, H.H. Abdalla, R.M. Ramadan, Ruthenium, osmium and rhodium-2,3-bis(2'-pyridyl)quinoxaline complexes, *Trans. Met. Chem.* 27 (2002) 69–74.
- [40] R. Bellam, D. Jaganyi, A. Mambanda, R. Robinson, Role of a 2,3-bis(pyridyl)pyrazinyl chelate bridging ligand in the reactivity of Ru(II)-Pt(II) dinuclear complexes on the substitution of chlorides by thiourea nucleophiles—a kinetic study, *New J. Chem.* 42 (2018) 12557–12569.
- [41] T.J. Whittemore, T.A. White, C. Turro, New ligand design provides delocalization and promotes strong absorption throughout the visible region in a Ru(II) complex, *J. Am. Chem. Soc.* 140 (2018) 229–234.
- [42] C. Zúñiga, I. Crivelli, B. Loeb, Synthesis, characterization, spectroscopic and electrochemical studies of donor-acceptor ruthenium(II) polypyridine ligand derivatives with potential NLO applications, *Polyhedron* 85 (2015) 511–518.
- [43] B.J. Coe, M.K. Peers, N.S. Scrutton, Syntheses and electronic and optical properties of complexes of the bis(2,2'-bipyrazyl)ruthenium unit, *Polyhedron* 96 (2015) 57–65.
- [44] C. Goze, C. Leiggener, S.X. Liu, L. Sanguinet, E. Levillain, A. Hauser, S. Decurtins, Fused donor-acceptor ligands in RuII chemistry: Synthesis, electrochemistry and spectroscopy of [Ru(bpy)3-n(TTF-dppz) n](PF6)2, *ChemPhysChem* 8 (2007) 1504–1512.
- [45] A. Ghosh, P. Das, M.R. Gill, P. Kar, M.G. Walker, J.A. Thomas, A. Das, Photoactive RuII-polypyridyl complexes that display sequence selectivity and high-affinity binding to duplex DNA through groove binding, *Chem. Eur. J.* 17 (2011) 2089–2098.
- [46] Y. Kim, A. Das, H. Zhang, P.K. Dutta, Zeolite membrane-based artificial photosynthetic assembly for long-lived charge separation, *J. Phys. Chem. B* 109 (2005) 6929–6932.
- [47] M. Milkevitch, E. Brauns, K.J. Brewer, Spectroscopic and electrochemical properties of a series of mixed-metal d6, d8 bimetallic complexes of the form [(bpy)2M(BL)PtC2]2+, (bpy = 2,2'-Bipyridine; BL = dpq (2,3-Bis(2-pyridyl) quinoxaline) or dpb (2,3-Bis(2-pyridyl)-benzoquinoxaline); M = O^SI or Ru^{II}), *Inorg. Chem.* 35 (1996) 1737–1739.
- [48] X. Ragàs, A. Jiménez-Banzo, D. Sánchez-García, X. Batllori, S. Nonell, Singlet oxygen photosensitisation by the fluorescent probe Singlet Oxygen Sensor Green, *Chem. Commun.* (20) (2009) 2920.
- [49] X. Chen, Z. Zhong, Z. Xu, L. Chen, Y. Wang, 2',7'-Dichlorodihydrofluorescein as a fluorescent probe for reactive oxygen species measurement: Forty years of application and controversy, *Free Radical Res.* 44 (6) (2010) 587–604.
- [50] G.H. Ribeiro, L. Colina-Vegas, J.C.T. Clavijo, J. Ellena, M.R. Cominetti, A. A. Batista, Ru(II)/N-N/PPH 3 complexes as potential anticancer agents against MDA-MB-231 cancer cells (N-N = diimine or diamine), *J. Inorg. Biochem.* 193 (2019) 70–83.
- [51] I. Gurgul, O. Mazuryk, M. Łomzik, P.C. Gros, D. Rutkowska-Zbik, M. Brindell, Unexplored features of Ru(II) polypyridyl complexes - towards combined cytotoxic and antimetastatic activity, *Metallomics* 12 (2020) 784–793.
- [52] O. Mazuryk, F. Suzenet, C. Kieda, M. Brindell, The biological effect of the nitroimidazole derivative of a polypyridyl ruthenium complex on cancer and endothelial cells, *Metallomics* 7 (3) (2015) 553–566.
- [53] P. Gajda-Morszewski, I. Gurgul, E. Janczy-Cempa, O. Mazuryk, M. Łomzik, M. Brindell, Inhibition of matrix metalloproteinases and cancer cell detachment by Ru(II) polypyridyl complexes containing 4,7-diphenyl-1,10-phenanthroline ligands—new candidates for antimetastatic agents, *Pharmaceuticals* 14 (10) (2021) 1014.
- [54] C. Zhang, B.J. Han, C.C. Zeng, S.H. Lai, W. Li, B. Tang, D. Wan, G.B. Jiang, Y.J. Liu, Synthesis, characterization, in vitro cytotoxicity and anticancer effects of ruthenium(II) complexes on BEL-7402 cells, *J. Inorg. Biochem.* 157 (2016) 62–72.
- [55] A. Florence Tikum, Y.J. Jeon, J.H. Lee, M.H. Park, I.Y. Bae, S.H. Kim, H.J. Lee, J. Kim, Cytotoxic and anticancer properties of new ruthenium polypyridyl complexes with different lipophilicities, *J. Inorg. Biochem.* 180 (2018) 204–210.
- [56] G.B. Jiang, W.Y. Zhang, M. He, Y.Y. Gu, L. Bai, Y.J. Wang, Q.Y. Yi, F. Du, Anticancer activity of two ruthenium(II) polypyridyl complexes toward Hepatocellular carcinoma HepG-2 cells, *Polyhedron* 169 (2019) 209–218.
- [57] M. Brindell, I. Gurgul, E. Janczy-Cempa, P. Gajda-Morszewski, O. Mazuryk, Moving Ru polypyridyl complexes beyond cytotoxic activity towards metastasis inhibition, *J. Inorg. Biochem.* 226 (2022) 111652.